Halo concentrations in the standard ΛCDM cosmology

Francisco Prada[1,2]⋆, Anatoly A. Klypin[3], Antonio J. Cuesta[1,4],
Juan E. Betancort-Rijo[5] and Joel Primack[6]

[1] *Instituto de Astrofisica de Andalucia (CSIC), E-18080 Granada, Spain*
[2] *Visiting Professor at the Institute for Computational Cosmology, Department of Physics, University of Durham, UK*
[3] *Astronomy Department, New Mexico State University, Las Cruces, NM, USA*
[4] *Present address: Yale Center for Astronomy and Astrophysics, Yale University, New Haven, CT, USA*
[5] *Instituto de Astrofisica de Canarias, Tenerife, Spain*
[6] *Department of Physics, University of California at Santa Cruz, Santa Cruz, CA, USA*

ABSTRACT

We study the concentration of dark matter halos and its evolution in N-body simulations of the standard ΛCDM cosmology. The results presented in this paper are based on 4 large N-body simulations with ~ 10 billion particles each: the Millennium-I and II, Bolshoi, and MultiDark simulations. The MultiDark (or BigBolshoi) simulation is introduced in this paper. This suite of simulations with high mass resolution over a large volume allows us to compute with unprecedented accuracy the concentration over a large range of scales (about six orders of magnitude in mass), which constitutes the state-of-the-art of our current knowledge on this basic property of dark matter halos in the ΛCDM cosmology. We find that there is consistency among the different simulation data sets, despite the different codes, numerical algorithms, and halo/subhalo finders used in our analysis. We confirm a novel feature for halo concentrations at high redshifts: a flattening and upturn with increasing mass. The concentration $c(M, z)$ as a function of mass and the redshift and for different cosmological parameters shows a remarkably complex pattern. However, when expressed in terms of the linear rms fluctuation of the density field $\sigma(M, z)$, the halo concentration $c(\sigma)$ shows a nearly-universal simple U-shaped behaviour with a minimum at a well defined scale at $\sigma \sim 0.71$. Yet, some small dependences with redshift and cosmology still remain. At the high-mass end ($\sigma < 1$) the median halo kinematic profiles show large signatures of infall and highly radial orbits. This c–$\sigma(M, z)$ relation can be accurately parametrized and provides an analytical model for the dependence of concentration on halo mass. When applied to galaxy clusters, our estimates of concentrations are substantially larger – by a factor up to 1.5 – than previous results from smaller simulations, and are in much better agreement with results of observations.

Key words: cosmology: theory – dark matter – galaxies: halos – methods: N-body simulations.

1 INTRODUCTION

N-body cosmological simulations have been essential for understanding the growth of structure in the Universe, and in particular, they have been crucial for studying the properties of dark matter halos in the standard Lambda Cold Dark Matter (ΛCDM) cosmology. Simulations are also an invaluable tool for analyzing galaxy surveys, for studying the abundance evolution of clusters of galaxies, and for semi-analytical models of galaxy formation. In recent years, the development of numerical codes and access to powerful supercomputers have made it possible to perform *Grand Challenge* cosmological simulations with high mass resolution over a large volume, which provide the basis to attack many problems in cosmology. The Millennium simulation (Springel et al. 2005, MS-I), its smaller volume and higher-resolution Millennium-II version (Boylan-Kolchin et al. 2009, MS-II) and the new Bolshoi simulation (Klypin et al. 2010), in this respect, constitute a remarkable achievement.

⋆ E-mail: fprada@iaa.es

Millennium, Bolshoi, and the new MultiDark (or Big-Bolshoi) simulation, which is introduced in this work, allow us to estimate for the ΛCDM cosmology, with unprecedented statistics, the concentration of dark matter halos and its evolution over six orders of magnitude in mass. The comparison between this suite of cosmological simulations also provides an unique opportunity to study consistency on dark matter halo statistics using different codes, numerical algorithms, halo finders and cosmological parameters. Halo concentrations $c \equiv R_{\rm vir}/r_s$ have been studied extensively during the last decade. Here $R_{\rm vir}$ is the virial radius of a halo and r_s is the break radius between an inner $\sim r^{-1}$ density profile and an outer r^{-3} profile. Typically, the median halo concentration declines with increasing mass and redshift (Bullock et al. 2001), and the shape of the mass–concentration median relation evolves. Recently, Klypin et al. (2010) found a novel feature: at high redshift, the concentration flattens, and then increases slightly for high masses. Numerous works made use of cosmological simulations to determine the correlation and scatter of concentration with halo mass, its evolution, and its dependence on environment and cosmology (e.g. Navarro, Frenk, & White 1997; Bullock et al. 2001; Eke, Navarro, & Steinmetz 2001; Wechsler et al. 2002; Zhao et al. 2003; Neto et al. 2007; Gao et al. 2008; Macciò, Dutton, & van den Bosch 2008; Zhao et al. 2009; Muñoz-Cuartas et al. 2010; Klypin et al. 2010). Moreover, the dependence of halo concentrations on their merging history has been studied also in detail. For example, Wechsler et al. (2002); Zhao et al. (2003, 2009) determine concentrations using accurate modeling of halo mass accretion histories. Simulations and analytical models have tried also to understand the formation and evolution of the central density cusp of dark matter halos - assuming that they grow inside out during the different phases in their mass accretion histories - to provide predictions on halo concentrations (see e.g. Reed et al. 2005; Lu et al. 2006; Romano-Díaz et al. 2007; Hoffman et al. 2007; Salvador-Solé et al. 2007). The origin of halo concentrations ultimately is linked to the physical process that yield the formation of the NFW density profiles in the cold dark matter scenario (see also Dalal, Lithwick, & Kuhlen 2010).

Here, we show that the dependence of concentration on halo mass and its evolution can be obtained from the *rms* fluctuation amplitude of the linear density field $\sigma(M, z)$ by using our new analytical model based on the concentration–$\sigma(M, z)$ relation. This model is able to reproduce all relevant features observed in the halo mass–concentration median relations at different redshifts: the decline of concentration with mass, its flattening and upturn.

In this paper, we study the evolution of halo concentrations in N-body cosmological simulations of a ΛCDM cosmology. We cover a large range of scales, going from halos hosting dwarf galaxies to massive galaxy clusters. This corresponds to halo maximum circular velocities ranging from 25 to 1800 km s^{-1}, covering six orders of magnitude in mass. In Section 2 we describe the simulations and halo catalogs used in this work. Methodology to estimate halo concentrations is presented in section 3. In this paper we analyze only distinct halos. A halo is called distinct if its center is not inside the virial radius of a larger halo. In Section 4 we study concentrations of distinct halos and their evolution

with redshift using data from the Millennium, Bolshoi and the new MultiDark simulations. A new parameterization of the distinct halo concentrations as a function of the *rms* of the linear density field $\sigma(M, z)$ is presented in Section 5. Main results of this work are summarized in Section 5. An Appendix gives discussion of various selection effects.

2   SIMULATIONS AND HALO IDENTIFICATION

Table 1 summarizes the basic numerical and cosmological parameters of the four simulations used in this work. The Millennium simulation (Springel et al. 2005) and the more recent Millennium-II simulation (Boylan-Kolchin et al. 2009) adopted the same WMAP first year cosmological parameters, used the same number of particles to resolve the density field, and share the same output data structure. MS-II was done in a cubic simulation box one-fifth the linear size of the original MS-I with 5 times better force resolution and 125 times better mass resolution. MS-I,II were run with the TREE-PM codes GADGET-2 and GADGET-3 respectively.

The Bolshoi (Klypin et al. 2010) and the MultiDark simulations use the latest WMAP5 and WMAP7 cosmological parameters, which are also consistent with other recent observational constraints – see Figure 1 of Klypin et al. (2010) . The Adaptive-Refinement-Tree (ART) code was used for these two simulations. ART is an Adaptive-Mesh-Refinement (AMR) type code. A detailed description of the code is given in Kravtsov et al. (1997) and Kravtsov (1999). The code was parallelized using MPI libraries and OpenMP directives (Gottloeber & Klypin 2008). Details of the time-stepping algorithm and comparison with GADGET and PKDGRAV codes are given in Klypin et al. (2009). The ART code increases the force resolution by splitting individual cubic cells into $2 \times 2 \times 2$ cells with each new cell having one half the size of its parent. This is done for every cell if the density of the cell exceeds some specified threshold. The value of the threshold varies with the level of refinement and with the redshift and is typically 2-5 particles per cell. 180 snapshots were saved for analysis. Details of the Bolshoi simulations are given in Klypin et al. (2010).

Here we give some details of the MultiDark run. Initial conditions were set at the redshift $z_{\rm init} = 65$ using the same power spectrum as for Bolshoi. The force resolution in the ART code varies with time. The *comoving* resolution (size of the smallest cell) for the MultiDark was equal to $244\,h^{-1}$kpc at $z > 10$. When the fluctuations started to collapse, the resolution became smaller and at $z = 0$ it was $7.6\,h^{-1}$kpc. The ART code is designed in such a way that the *proper* (physical) resolution is nearly preserved over time. For MultiDark the proper resolution was $\sim 7\,h^{-1}$kpc for $z = 0 - 8$ as compared with $1\,h^{-1}$kpc for $z = 0 - 20$ for Bolshoi. The total volume resolved at the highest resolution at $z = 0$ was $360(h^{-1}{\rm Mpc})^3$ and $2.8 \times 10^4(h^{-1}{\rm Mpc})^3$ for twice worse resolution. 50 snapshots were saved for analysis.

The main difference in cosmological parameters between the simulations is that the Millennium simulations adopted a substantially larger amplitude of perturbations σ_8 that is nearly 4σ away from recent constraints (e.g., Klypin et al. 2010; Guo et al. 2011). The difference is even larger on galaxy scales since the Millennium simulations

used a larger tilt n_s of the power spectra (see Table 1, and Figure 2 in Klypin et al. (2010) for the comparison of the linear power spectra of Bolshoi and Millennium simulations).

In this paper we analyze only distinct halos. A halo is called distinct if its center is not inside the virial radius of a larger halo. One of the most important characteristics of a halo is its maximum circular velocity:

$$V_{\max}^2 = \max \left[\frac{GM(<r)}{r} \right]. \qquad (1)$$

There are several advantages of using $V_{\max}$ to characterize a halo as opposed to the virial mass. First, $V_{\max}$ does not have the ambiguity related with the definition of "virial mass." Virial mass and radius vary depending on overdensity threshold used. For the often-employed overdensity 200 and "virial" overdensity thresholds, the differences in definitions result in changes in the halo radius from one definition to another and, thus, in concentration, by a factor of 1.2-1.3, with the exact value being dependent on the halo concentration. Second and more important, the maximum circular velocity $V_{\max}$ is a better quantity to characterize halos when we relate them to the galaxies inside these halos. For galaxy-size halos the maximum circular velocity is defined at a radius of ~ 40 kpc: closer to sizes of luminous parts of galaxies than the much larger virial radius, which for the Milky-Way halo is ~ 250 kpc (e.g., Klypin et al. 2002).

In both Millennium simulations dark matter halos were found using the friends-of-friends algorithm (FOF, Davis et al. 1985), with a linking length of $b = 0.2$. The SUBFIND code (Springel et al. 2001) searched for bound substructures within every FOF group. In most cases, the main component of a FOF group is typically a dominant spherical "subhalo" whose particles make up most of the bound component of the FOF group. This dominant or central subhalo can be identified as a distinct halo with a maximum circular velocity $V_{\max}$. For our analysis we consider all distinct halos (i.e. dominant subhalos of FOF groups) with maximum circular velocities greater than $V_{\max} > 25 \, \mathrm{km \, s^{-1}}$ and $V_{\max} > 70 \, \mathrm{km \, s^{-1}}$ for MS-II and MS-I respectively. Halo velocity functions are complete above these velocities (see Springel et al. 2005; Boylan-Kolchin et al. 2009). We have downloaded[1] MS-I and MS-II halo catalogs for several epochs up to $z = 10$, as close as possible to those redshifts available for Bolshoi and MultiDark.

Dark matter halos are identified in Bolshoi and Multi-Dark with a parallel version of the Bound-Density-Maxima (BDM) algorithm (Klypin & Holtzman 1997). The BDM is a Spherical Overdensity (SO) code. It finds all density maxima in the distribution of particles using a top-hat filter with 20 particles. For each maximum the code estimates the radius within which the overdensity has a specified value. Among all overlapping density maxima the code finds one that has the deepest gravitational potential. The position of this maximum is the center of a distinct halo[2].

The halo radius can be defined as the radius of a sphere within which the average density is Δ times larger than the
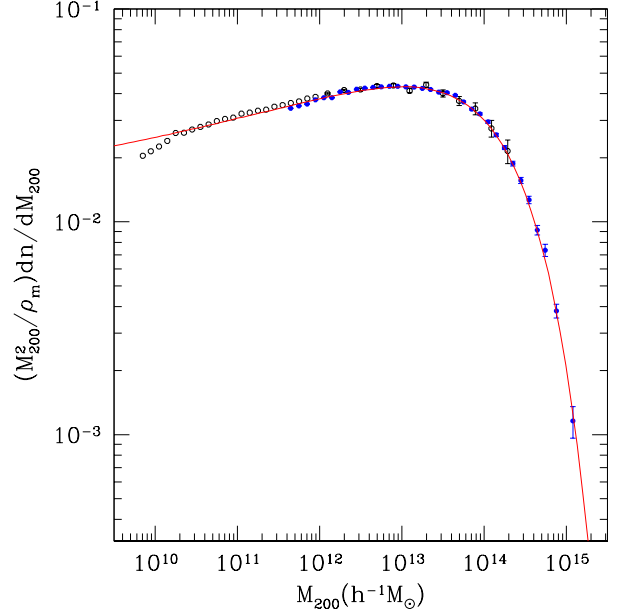
Figure 1. Mass functions of distinct halos in Bolshoi (open circles) and MultiDark (filled circles) simulations at $z = 0$. The analytical approximation of Tinker et al. (2008) is shown by the curve. In the overlapping region both simulations produce nearly identical results.

critical density of the Universe:

$$M = \frac{4\pi}{3} \Delta \rho_{\mathrm{cr}}(z) R^3, \qquad (2)$$

where $\rho_{\mathrm{cr}}(z)$ is the critical density of the Universe. In this paper we use the overdensity $\Delta = 200$ threshold. Corresponding values for mass and radius are $M = M_{200}$ and $R = R_{200}$.

Figure 1 shows differential mass functions of distinct halos in Bolshoi and MultiDark simulations. The two simulations demonstrate remarkably good consistency in the overlapping region of masses $(10^{12} - 10^{14})h^{-1}M_\odot$. To describe the mass function dn/dM we use the following equations:

$$\frac{dn}{dM} = f(\sigma)\frac{\rho_m}{M}\frac{d\log \sigma^{-1}}{dM}, \qquad (3)$$

$$f(\sigma) = A\left[1 + \left(\frac{\sigma}{b}\right)^{-a}\right]\exp\left(-\frac{c}{\sigma^2}\right), \qquad (4)$$

$$\sigma^2(M,z) = \frac{1}{2\pi^2}\int_0^\infty P(k,z)W^2(k,M)k^2 dk, \qquad (5)$$

where ρ_m is the cosmological matter density, and $P(k,z)$ is the power spectrum of fluctuations. Here $\sigma(M,z)$ is the linear rms fluctuation of density field on the scale M as estimated with the top-hat filter, whose Fourier spectrum is $W(k,M)$. Parameters of the approximation are nearly the same as in Tinker et al. (2008) for the same overdensity Δ: $A = 0.213$, $a = 1.80$, $b = 1.85$, and $c = 1.57$.

Analysis of halo concentrations is done for different populations of halos. We limit our analysis to halos containing more than 500 particles. Most of the time we analyze all such halos regardless of their degree of virialization or interaction. Occasionally we select only "relaxed" halos. A number of parameters is involved in this selection. We de-

Table 1. Basic parameters of the cosmological simulations. L_{box} is the side length of the simulation box, N_p is the number of simulation particles, ϵ is the force resolution in comoving coordinates, M_p refers to the mass of each simulation particle, and the parameters Ω_m, Ω_Λ, Ω_b, n_s (the spectral index of the primordial power spectrum), h (the Hubble constant at present in units of 100 $km/sMpc^{-1}$) and σ_8 (the rms amplitude of linear mass fluctuations in spheres of 8 $h^{-1}Mpc$ comoving radius at redshift $z = 0$) are the ΛCDM cosmological parameters assumed in each simulation.

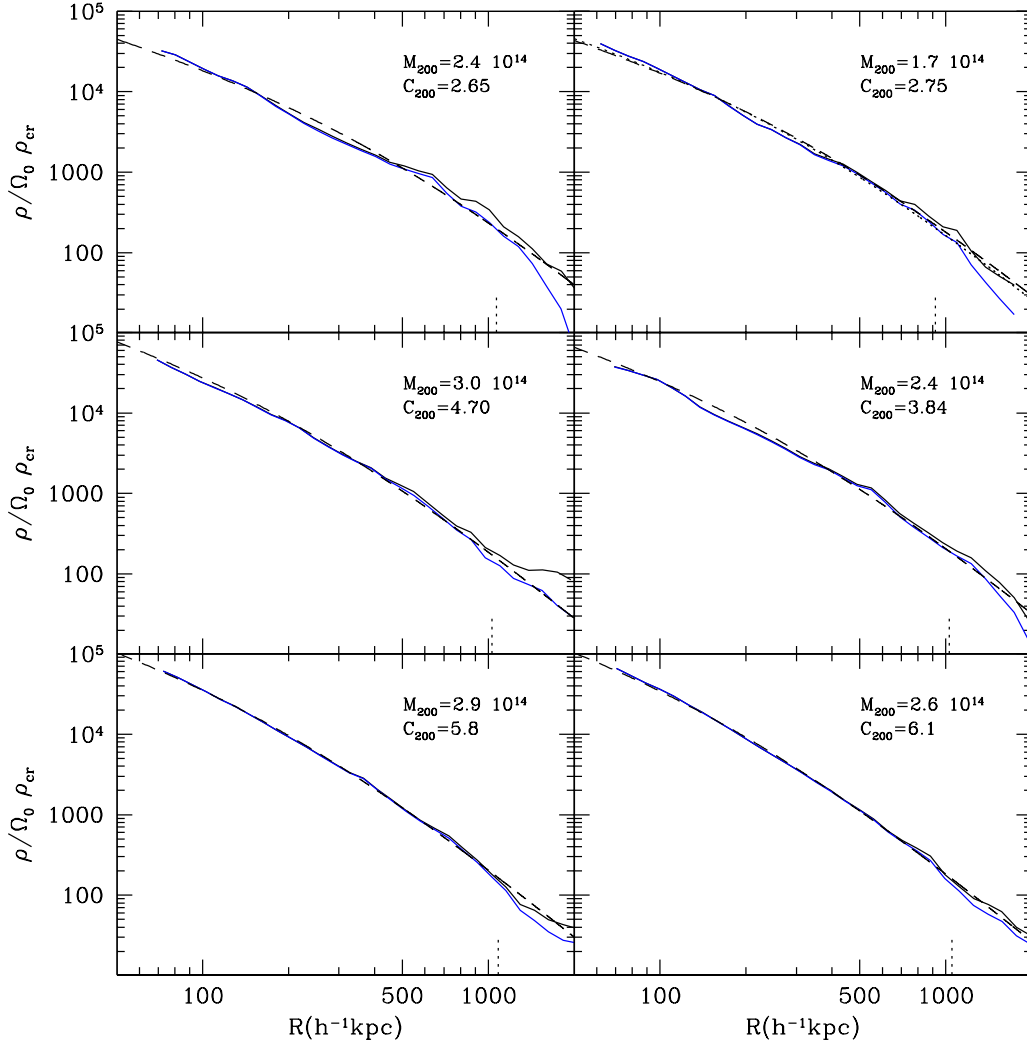| Name	L_{box} $(h^{-1}\mathrm{Mpc})$	N_p	ϵ $(h^{-1}\mathrm{kpc})$	M_p $(h^{-1}M_\odot)$	Ω_m	Ω_Λ	Ω_b	n_s	h	σ_8	reference
Millennium	500	2160^3	5	$8.61\,10^8$	0.25	0.75	0.0450	1.00	0.73	0.90	Springel et al. 2005
Millennium-II	100	2160^3	1	$6.89\,10^6$	0.25	0.75	0.0450	1.00	0.73	0.90	Boylan-Kolchin et al. 2009
Bolshoi	250	2048^3	1	$1.35\,10^8$	0.27	0.73	0.0469	0.95	0.70	0.82	Klypin et al. 2010
MultiDark	1000	2048^3	7	$8.63\,10^9$	0.27	0.73	0.0469	0.95	0.70	0.82	this work

Figure 3. Examples of halo density profiles (full curves) and their fits (dashed curves) using concentrations obtained with the ratios of the maximum circular velocity $V_{\max}$ to the halo velocity V_{200}. Each panel shows two full curves: the density profile of all particles (upper curve) and only bound particles (lower curve). Vertical dotted lines show the outer radius of bound particles. Typically the highly concentrated and relaxed halos are well fit by the approximations (two bottom panels). Low concentrated halos and halos with large perturbations (two top panels) show large deviations between the data and approximations. Fitting those unrelaxed profiles with standard minimization technique does not improve the accuracy of the fits as indicated by dotted curve in the top-right panel.
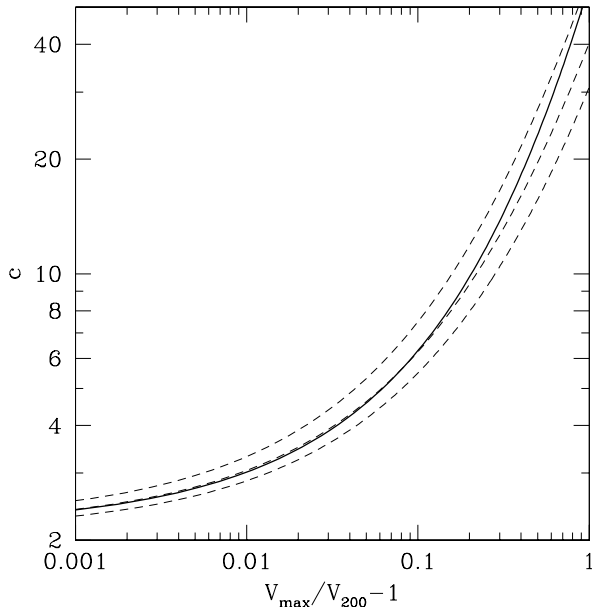
Figure 2. Relation between halo concentration c and the ratio of the maximum circular velocity $V_{\max}$ to the circular velocity at the virial radius V_{200} for the NFW profile (full curve) and for three Einasto profiles with parameters $\alpha = 0.15, 0.20, 0.25$ (from top to bottom).

fine an offset parameter $x_{\rm off}$ as the distance between the center of a halo (density maximum with the deepest gravitational potential) and the center of mass of the halo in units of the virial radius. For each halo we also use the spin parameter λ and the virial ratio $2K/|U| - 1$, where K and U are the total kinetic and potential energies. A halo is called "relaxed" if it satisfies the following three conditions: $x_{\rm off} < 0.1$, $2K/|U| - 1 < 0.5$, and $\lambda < 0.1$. Neto et al. (2007) and Macciò, Dutton, & van den Bosch (2008) give detailed discussion of these conditions.

3 FINDING HALO CONCENTRATIONS

There are different ways to estimate halo concentration. Traditionally it is done first by fitting a NFW profile

$$\rho_{\rm NFW} = \frac{4\rho_s}{x(1+x)^2}, \quad x \equiv \frac{r}{r_s} \tag{6}$$

to the spherically averaged density profile of a halo, where ρ_s and r_s are the characteristic density and radius. Then the halo concentration is found as the ratio of the virial radius to the characteristic radius r_s:

$$c = \frac{R_{200}}{r_s} \tag{7}$$

However, the fitting can be difficult. For example, special attention should be paid to the central region: if fitting starts too close to the center where the resolution is not sufficient, the fitting will produce too low concentration because the density in the center is underestimated. In addition to the problems with the center and the necessity to deal with binned data, direct fitting has another feature: it heavily relies on an assumption of a particular shape of the halo profile, which is typically taken as the NFW profile.

Halo profiles on average show systematic deviations from the NFW approximation and are better approximated with the Einasto profile (Navarro et al. 2004; Gao et al. 2008; Navarro et al. 2010). One may naively expect that fitting a more accurate approximation would produce better results on concentrations. This is not the case. There is a reason why halo concentrations are not estimated with the Einasto profile: results show large fluctuations in the concentration, which are due to a smaller curvature of density profile $\rho(r)$ in the crucial range of radii around the radius with the logarithmic slope -2. These weaknesses of the direct fitting provide a motivation to look for alternatives.

The idea is to start with the NFW profile. It is uniquely defined by the characteristic density ρ_s and the characteristic radius r_s. Instead of these two parameters one can use any two independent quantities to define the profile. For example, one can choose the virial radius and the radius at which the circular velocity reaches half of its maximum value as in Alam et al. (2002). Or one can use the radius containing 1/5 of virial mass and the virial mass (Avila-Reese et al. 1999). Recently Klypin et al. (2010) proposed to use a relation between the maximum circular velocity $V_{\max}$, the virial mass and the virial radius to estimate the halo concentration. We follow this idea and use a more simple version with parameters $V_{\max}$ and the circular velocity at the virial radius:

$$V_{200} = \left(\frac{GM_{200}}{R_{200}} \right)^{1/2}. \tag{8}$$

In this case the ratio $V_{\max}/V_{200}$ of the maximum circular velocity $V_{\max}$ to the virial velocity V_{200} is directly related with the halo concentration and can easily be interpreted because larger ratios imply larger concentration. The value of the halo concentration can be estimated by assuming a shape of the density profile. However, this is not required because the velocity ratio is a measure of the halo concentration regardless of what profiles halos have. For the case of the NFW halo density profile, the $V_{\max}/V_{200}$ velocity ratio is given by the following relation:

$$\frac{V_{\max}}{V_{200}} = \left(\frac{0.216\,c}{f(c)} \right)^{1/2}, \tag{9}$$

where $f(c)$ is

$$f(c) = \ln(1+c) - \frac{c}{(1+c)}. \tag{10}$$

Having the $V_{\max}/V_{200}$ ratio for each halo, we find the halo concentration c by solving numerically eqs. (9 - 10). For convenience, Figure 2 shows the dependence of concentration c on $V_{\max}/V_{200}$ in a graphical form. We also present results for three typical Einasto profiles (Navarro et al. 2004; Gao et al. 2008; Navarro et al. 2010):

$$\rho_{\rm Ein} = \rho_s \exp \left[-\frac{2}{\alpha} \left(x^\alpha - 1 \right) \right], \quad x \equiv \frac{r}{r_s}. \tag{11}$$

In practice we bin halos by their *maximum circular velocity* $V_{\max}$. At a given redshift and for each circular velocity bin we obtain the *median* virial velocity V_{200}. Then we compute c by solving eqs. (9 - 10).

We made different tests of the accuracy of our algorithm. We find quite a good agreement of our estimates of c with the results of direct fitting of halo profiles by Neto et al.
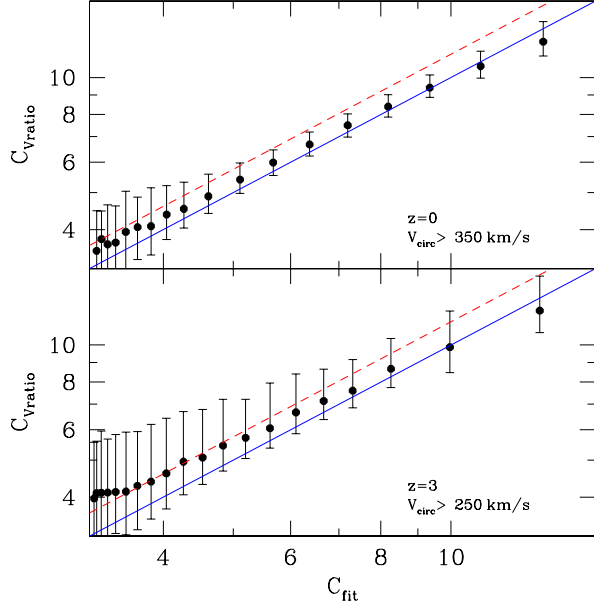
Figure 4. Comparison of halo concentrations c_{fit} obtained by fitting the NFW profiles to halo densities with concentrations c_{Vratio} found using the ratios of the maximum circular velocity V_{max} to the halo velocity V_{200}. The most massive ~ 10000 halos in the Bolshoi simulation are used for the plot. The top (bottom) panel shows halos at $z = 0$ ($z = 3$). All halos are used regardless of their relaxation status. Full lines present the relation $c_{\text{Vratio}} = c_{\text{NFWfit}}$. The dashed lines show a 15% offset between the two concentrations. Most of the median concentrations fall between those two lines. Error bars present 10 and 90 percent spread of the distribution of individual concentrations.

(2007) with the deviations between the two methods being less than 5 percent for the whole range of masses in the MS simulation. Figure 3 shows six examples of fitting density profiles of large halos with $M_{200} \approx (1.5 - 3) \times 10^{14} h^{-1} M_\odot$ in the Bolshoi simulation. Each of the halos is resolved with more than a million particles and the random noise associated with finite number of particles is practically negligible. We use 30 radial bins equally spaced in logarithm of radius with $\Delta \log(r/R_{200}) = 0.05$ up to $R = 2R_{200}$. Plots show typical examples of high and low concentration halos. Just as expected, for halos with smooth density profiles (the bottom row of panels) the accuracy of fits obtained with V_{max}/V_{200} concentrations is very good. Halos with large substructures and big radial fluctuations (typically halos with low concentration; the top row of panels) result in relatively poor fits. However, in these cases the direct fitting does not produce much better approximations as demonstrated by the top right panel.

Figure 4 provides a more extensive comparison of concentrations obtained with the direct fitting and with the V_{max}/V_{200} ratio method. For this plot we select all ~ 7000 halos in the Bolshoi simulation with $V_{\text{max}} > 350\,\text{km s}^{-1}$ at $z = 0$ and ~ 10000 halos with $V_{\text{max}} > 250\,\text{km s}^{-1}$ at $z = 3$. The halos with concentration larger than $c \approx 5$ demonstrate a tight relation between the two estimates of concentration: more than 90 percent of halos fall between two lines: $c_{\text{Vratio}} = c_{\text{fit}}$ and $c_{\text{Vratio}} = 1.15c_{\text{fit}}$. At smaller concentrations
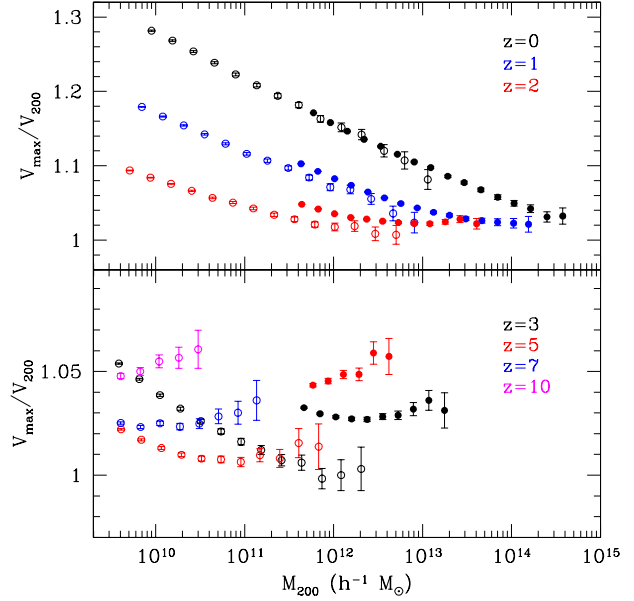

Figure 5. The ratio V_{max}/V_{200} of the maximum circular velocity to the virial velocity as a function of mass M_{200} for distinct halos at different redshifts for MS-I (filled symbols) and MS-II (open symbols) simulations. Error bars are statistical uncertainties. The MS-I and MS-II simulations agree quite well at $z = 0$. At higher redshifts there are noticeable differences between MS-I and MS-II.

there is a small systematic (5-15)% offset between the two estimates.

These results demonstrate that both the direct fitting of density profiles and the method based on the V_{max}/V_{200} ratio give similar concentrations. There are the small systematic deviations, which for relaxed halos or for halos with concentrations $c > 5$ are less than a few percent. For halos with small concentrations the deviations are larger, but are still less than $\sim 15\%$. We ignore these differences and use concentrations based on the V_{max}/V_{200} ratios.

4   EVOLUTION OF THE DISTINCT HALO CONCENTRATIONS WITH REDSHIFT: RESULTS OF SIMULATIONS

Our analysis of halo concentrations in different simulations starts with the simpler statistics of V_{max}/V_{200}. It is directly related with the concentration c, but V_{max}/V_{200} does not require an assumption of a particular density profile. These raw data are presented in Figures 5-6 for all simulations discussed in section 2. Here we consider only halos with more than 500 particles for our analysis. Error bars correspond to the statistical uncertainty in the determination of the V_{max}/V_{200} median velocity ratio. Halos are binned by V_{max}, and the average M_{200} for each velocity bin is the horizontal axis.

At $z = 0$, the agreement between both Millennium simulations is very good in the range of masses where they overlap. This is expected if the two simulations faithfully present results of the cosmological model and are not affected by finite box sizes or any other numerical issues. Yet, at higher redshifts there are notable differences between MS-
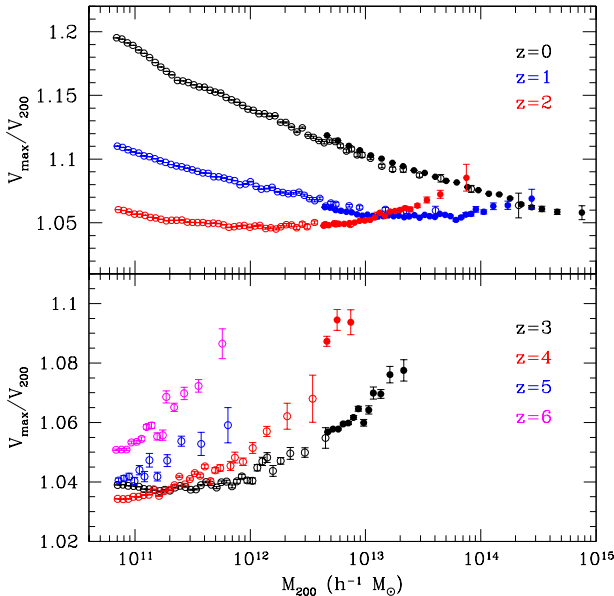
Figure 6. The same as Figure 5 but for Bolshoi (open symbols) and MultiDark (filled symbols) simulations. Both simulations show remarkable agreement at all masses and redshifts.

I and MS-II (see Figure 5). At a fixed halo mass M_{200}, data from MS-I yield systematically larger V_{max}/V_{200} velocity ratios, increasing with redshift up to a $3-4\%$ difference. For example, at $z=3$ we find $\sim 3\%$ difference for $10^{12}h^{-1}M_{\odot}$. This will translate to a difference of about $20-40\%$ in terms of halo concentration according to eq. (9).

Regardless of this discrepancy between the two Millennium simulations, we do clearly see an upturn of the velocity ratios, and, hence, halo concentrations with increasing halo mass at higher redshifts. The same is observed in the Bolshoi and MultiDark simulations (see Figure 6). We conclude that concentrations of distinct halos do increase with halo mass at higher redshifts as previously reported by Klypin et al. (2010). In spite of the qualitative agreement, there are differences between Bolshoi/MultiDark and the Millennium-I/II simulations. Those are expected and are due mainly to the different cosmological parameters used in the simulations.

The reason for the discrepancy between Millennium simulations found in the V_{max}/V_{200} velocity ratios at high redshifts is not clear. It might be due to differences in mass and force resolution. If that were true, one may expect that a lower resolution MS-I simulation should have a lower concentration. However, this is not the case: MS-I has larger concentration for overlapping masses. An important aspect that could cause this discrepancy is the fact that substructure within the dominant (distinct) halo is not taken into account when V_{max} is computed. Certainly this could make differences up to the level of few percent as observed. The MultiDark simulation is helping us to clarify this issue because MultiDark and Bolshoi have very different resolutions. In this case, we do see in Figure 6 a good agreement with the Bolshoi simulation at all redshifts in the mass interval where both simulations overlap. The BDM halo finder does include substructures within distinct halos to compute V_{max}.

So far we were following the traditional path of studying concentrations by expressing results for c as functions of halo
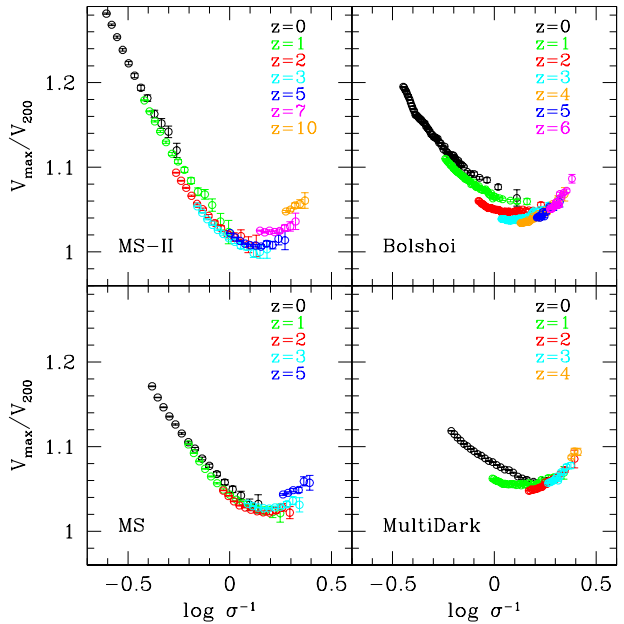

Figure 7. The ratio V_{max}/V_{200} as a function of $\log \sigma^{-1}$. In this plot halos mass increases from left to right. The large variations in shapes and amplitudes of $V_{max}/V_{200} - M$ seen in Figures 5-6 are replaced with much tighter relations $V_{max}/V_{200} - \log \sigma^{-1}$. All simulations show the same pattern: V_{max}/V_{200} has a U-shape with an upturn at large masses.

mass at different redshifts $c = c(M,z)$ (e.g., Bullock et al. 2001; Eke, Navarro, & Steinmetz 2001; Zhao et al. 2003; Macciò, Dutton, & van den Bosch 2008). As many other groups find, results for $c(M,z)$ appear to be not simple: the concentration evolves in a complicated way. In addition to previously found effects, at high redshifts the amplitude starts to increase, which makes the whole $c(M,z)$ function very complex.

One of reasons why $c(M,z)$ may *look* too complicated is because "wrong" physical quantities M and z are used. The situation may be compared to the studies of the halo mass function. Once a more physical variable $\sigma(M,z)$ was used (see e.g. Jenkins et al. 2001; Sheth & Tormen 2002; Warren et al. 2006; Tinker et al. 2008), the results became more transparent. In turn, this simplification allowed the development of accurate approximations such as that presented by eqs. (3-5). We will follow the same direction when we study the halo concentration. In particular, as the main variable we choose $\log \sigma^{-1}(M,z)$ - a quantity that is widely used in the mass function analysis. Using this variable helps to remove most of the evolution of the concentration with redshift, helps to understand the differences due to the cosmological parameters and the matter power spectrum, and allows a more clear comparison between different simulations.

Figure 7 shows the V_{max}/V_{200} velocity ratio as a function of $\log \sigma^{-1}$ of distinct halos at different redshifts for both Millennium simulations (left panels) and Bolshoi/MultiDark (right panels). Large volume simulations MS-I & MultiDark provide good statistics at the high-mass end ($\log \sigma^{-1} > 0$) and the smaller boxes, with much higher numerical resolution (MS-II and Bolshoi), help to reach small values of
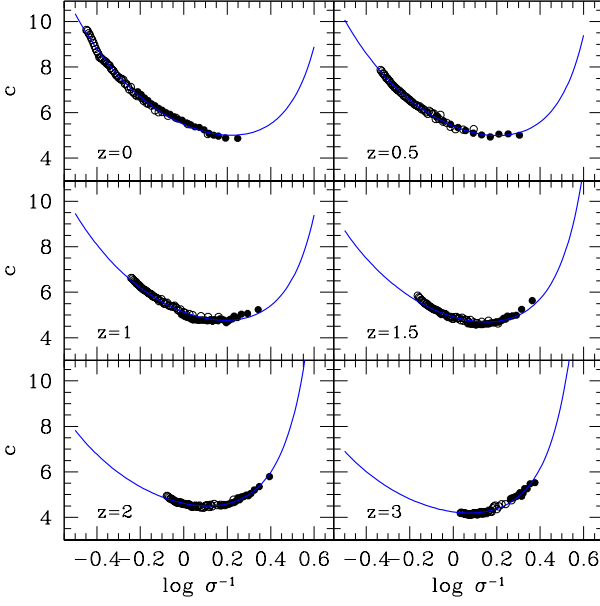
Figure 8. Concentration-$\sigma(M)$ median relation for distinct halos in the Bolshoi (open symbols) and MultiDark (filled symbols) simulations for different redshifts. Solid lines are predictions from our analytical model given by eqs.(14- 17). The data at different redshifts look very similar, but actually have a slight evolution: the minimum of c becomes smaller and it is reached at smaller $\log \sigma^{-1}$

$\log \sigma^{-1} < 0$ (small masses). Figure 7 also shows that when expressed in terms of the variable $\log \sigma^{-1}$, the concentration becomes a well-behaved function with an U shape: at low $\log \sigma^{-1}$ it decreases with $\log \sigma^{-1}$. Then it reaches a minimum at a well defined scale $\log \sigma^{-1} \approx 0.15$ ($\sigma \approx 0.707$), and at larger $\log \sigma^{-1}$ it begins to increase.

In spite of the fact that the rescaling from M to $\log \sigma^{-1}$ significantly reduces deviations in $V_{\max}/V_{200}$ (and, thus, in concentration), it does not completely remove all the deviations. There is still some residual dependence on cosmology: there are differences between the Millennium and the Bolshoi/MultiDark simulations. In addition, there is a weak evolution with redshift, which is more pronounced in high resolution runs Bolshoi and MS-II

As discussed above, at high redshifts there is a discrepancy between MS-I and MS-II simulations resulting in a $20 - 40\%$ difference in concentrations for a given halo mass M between the two simulations. At the same time, the overlap between Bolshoi and MultiDark is good at all redshifts. This is the reason we use Bolshoi and MultiDark to study the weak evolution of the $c - \log \sigma^{-1}$ relation with the redshift. The time evolution of the concentration can be described as a decrease of the minimum value of the U-shaped concentration curves with increasing redshift (from 5.1 at $z = 0$ down to 3.7 at $z = 4$), and a slight shift of the position of the minimum to smaller values of $\log \sigma^{-1}$, i.e. from 0.2 at $z = 0$ to 0.05 at $z = 4$. Figure 8 shows details of this weak evolution.

The nature of the upturn in the halo concentrations is an interesting problem on its own. We do not make detailed analysis of halos in the upturn, but we test some sim-
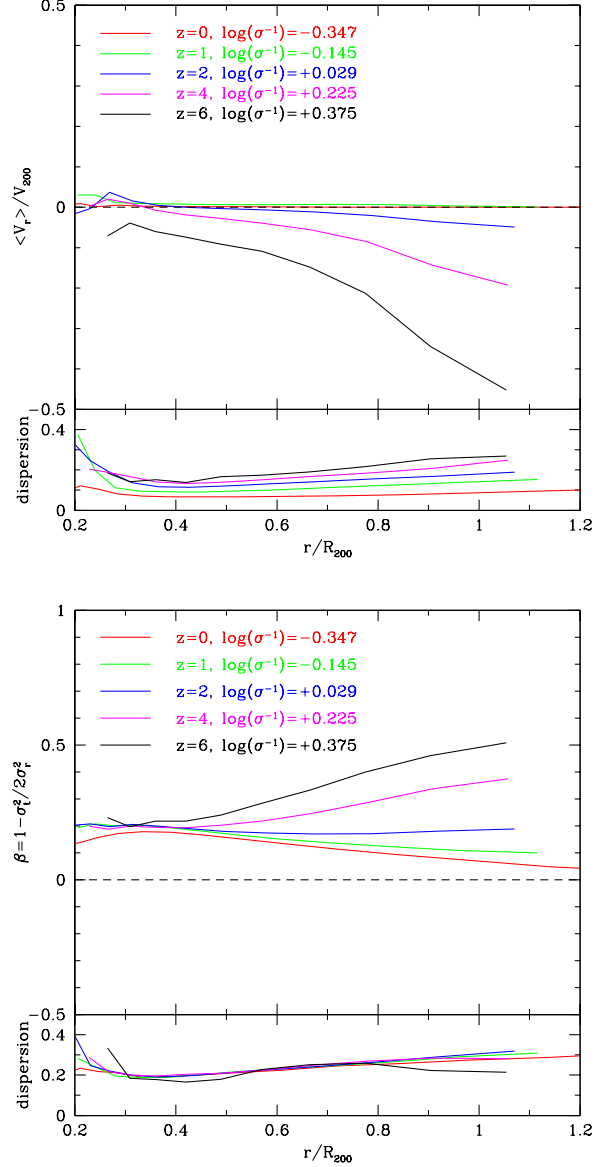

Figure 9. Average radial velocity $\langle V_r \rangle$ (top panels) and velocity anisotropy β (bottom panels) profiles for distinct halos selected from the Bolshoi simulation in different bins of $\log \sigma^{-1}$ and redshifts indicated in the plots. Halos with large $\log \sigma^{-1}$ (most massive halos) clearly show preferentially radial orbits and overall infall pattern at large distances from the halo center. Less massive halos ($\log \sigma^{-1} < 0$) on average do not have infall velocities and their orbits in the peripheral regions tend to be isotropic while retaining slightly radial velocities in the central regions.

ple hypotheses. One may think that the upturn is due to non-equilibrium effects. Indeed, the halos in the upturn are the largest halos at any given moment, and those halos are known to grow very fast. Results presented in the Appendix clearly show that out-of-equilibrium effects do not provide an explanation for the upturn: selecting relaxed halos only increases the magnitude of the upturn. However, the fast growth of the halos in the upturn does change the structure of the most massive halos (even those that are "relaxed").

Figure 9 shows average radial velocity profiles $\langle V_r \rangle$ and

velocity anisotropy β profiles for distinct halos in the Bolshoi simulation for different bins of log σ^{-1}. These statistics can be used to indicate the dynamical state of halos that lie at different locations in the $V_{\max}/V_{200}$–$\sigma(M)$ median relations displayed in Figure 7. Average halos in the high-mass end (i.e. log $\sigma^{-1} > 0$) clearly show signatures of infall given by large negative radial velocities. This is more clearly seen when expressed in terms of $\langle V_r \rangle$, but is also present in the velocity anisotropy $\beta = 1 - \sigma_t^2/2\sigma_r^2$, which tends to be larger at large values of log σ^{-1}. These results indicate that orbits are preferentially radial for halos in the upturn part of the $c - M$ relation. The situation changes for halos with smaller log σ^{-1}. They do not show an infall pattern and their velocity anisotropy is significantly smaller. Density profiles are less sensitive to these effects. The halos are "normal": on average they are well described by NFW for all log σ^{-1} bins. The only indication that something is not normal is the large halo concentration.

5   THE $C - \sigma(M)$ RELATION: AN ANALYTICAL MODEL FOR THE HALO MASS–CONCENTRATION RELATION

It is then desirable to provide for the ΛCDM cosmology an approximation that describes the dependence of halo concentration c on halo mass and redshift. However, approximations which use mass and redshift as the main variables are prone to a severe problem: lack of scalability. An approximation found for one set of cosmological parameters and for one particular redshift is not applicable to another cosmology or redshift. Just as with the mass function, we find a dramatic improvement of the accuracy of the approximations for the halo concentration once we use $\sigma(M,z)$. Following the same line of ideas, we use a new "time variable" x defined below. The motivation comes from the linear growth rate D of fluctuations in the ΛCDM cosmology. If it is normalized to be unity at $z = 0$, then

$$D(a) = \frac{5}{2}\left(\frac{\Omega_{\mathrm{m},0}}{\Omega_{\Lambda,0}}\right)^{1/3}\frac{\sqrt{1+x^3}}{x^{3/2}}\int_0^x \frac{x^{3/2}dx}{[1+x^3]^{3/2}}, \qquad (12)$$

$$x \equiv \left(\frac{\Omega_{\Lambda,0}}{\Omega_{\mathrm{m},0}}\right)^{1/3} a, \quad a \equiv (1+z)^{-1}, \qquad (13)$$

where $\Omega_{\mathrm{m},0}$ and $\Omega_{\Lambda,0}$ are the matter and cosmological constant density contributions at $z = 0$. Note that when D is written in this form, there is no explicit dependence on the redshift z: the time dependence goes through the variable x.

If the concentration c depended only on σ, we would had a universal function $c(\sigma)$. Similar to the mass function, we find that concentration is not universal and has some dependance on the redshift. We attribute this residual redshift dependence of $c(\sigma, a)$ mostly to the change in the growth rate of fluctuations $D(a)$ related to the change of matter density parameter $\Omega_{\mathrm{m}}(a)$. Another possible factor is the change with the redshift of the slope of the power spectrum $P(k)$ at a given σ. We find that corrections due to the growth rate factor produce sufficiently accurate fits and we do not study here the effect due to change in the $P(k)$ slope.

Because all our approximations use only σ and x, we *expect* that they are applicable also for different redshifts
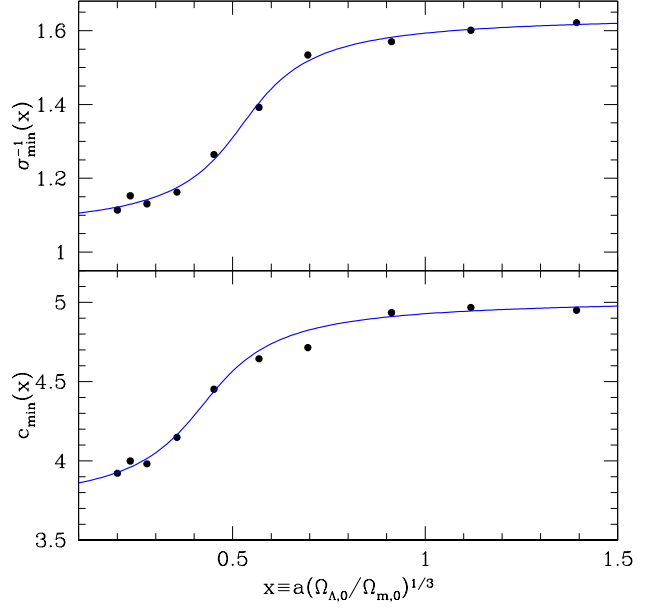

Figure 10. Dependence of the halo minimum concentration $c_{\min}$ (bottom panel) and the value of $\sigma_{\min}^{-1}$ (top panel) on x for distinct halos in the Bolshoi and MultiDark simulations. Solid lines are the approximations given in eqs.(19- 20).

and different cosmological parameters. Fitting of all available data from Bolshoi and MultiDark simulations gives the following approximation for halo concentration:

$$c(M,z) = B_0(x)\,\mathcal{C}(\sigma'), \qquad (14)$$

$$\sigma' = B_1(x)\,\sigma(M,x), \qquad (15)$$

$$\mathcal{C}(\sigma') = A\left[\left(\frac{\sigma'}{b}\right)^c + 1\right]\exp\left(\frac{d}{\sigma'^2}\right), \qquad (16)$$

where

$$A = 2.881,\ b = 1.257,\ c = 1.022,\ d = 0.060 \qquad (17)$$

The parameterization form of the function was motivated by the Sheth-Tormen (Sheth & Tormen 2002) approximation for the halo mass function. Here, the functions $B_0(x)$ and $B_1(x)$ are defined in such a way that they are equal to unity at $z = 0$ for the WMAP-5 parameters of the Bolshoi and MultiDark simulations. Thus, the function $\mathcal{C}(\sigma')$ is the concentration at $z = 0$ for this cosmological model. We find the following approximations for $B_0(x)$ and $B_1(x)$:

$$B_0(x) = \frac{c_{\min}(x)}{c_{\min}(1.393)}, \quad B_1(x) = \frac{\sigma_{\min}^{-1}(x)}{\sigma_{\min}^{-1}(1.393)}, \qquad (18)$$

where $c_{\min}$ and $\sigma_{\min}^{-1}$ define the minimum of the halo concentrations and the value of σ at the minimum:

$$c_{\min}(x) = c_0 + (c_1 - c_0)\left[\frac{1}{\pi}\arctan\left[\alpha(x - x_0)\right] + \frac{1}{2}\right] \quad (19)$$

$$\sigma_{\min}^{-1}(x) = \sigma_0^{-1} + (\sigma_1^{-1} - \sigma_0^{-1})\left[\frac{1}{\pi}\arctan\left[\beta(x - x_1)\right] + \frac{1}{2}\right], \quad (20)$$

where

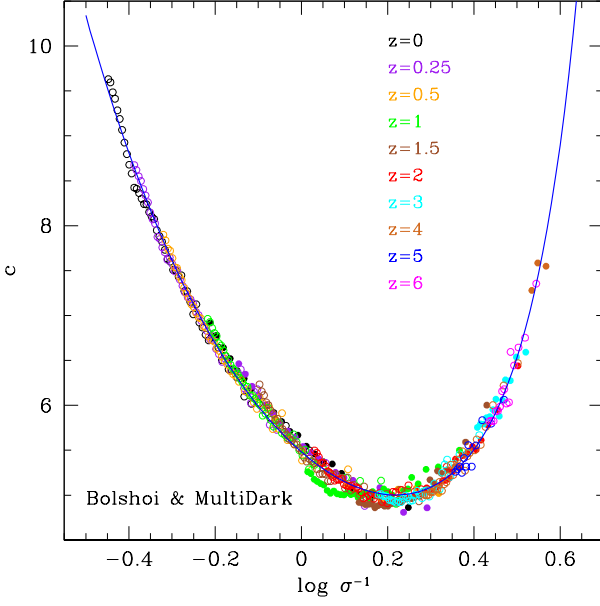$$c_0 = 3.681,\ c_1 = 5.033,\ \alpha = 6.948,\ x_0 = 0.424, \qquad (21)$$

Figure 11. Dependence of halo concentration c on $\log \sigma^{-1}$ after rescaling all the results of Bolshoi and MultiDark simulations to $z = 0$. The plot shows a tight intrinsic correlation of $\mathcal{C}$ on σ'.

and

$$\sigma_0^{-1} = 1.047, \ \sigma_1^{-1} = 1.646, \ \beta = 7.386, \ x_1 = 0.526. \quad (22)$$

Accurate approximations for the *rms* density fluctuation $\sigma(M, a)$ for the cosmological parameters of the Bolshoi/MultiDark simulations are given in Klypin et al. (2010) and for convenience are reproduced here:

$$\sigma(M, a) = D(a) \frac{16.9 \, y^{0.41}}{1 + 1.102 \, y^{0.20} + 6.22 \, y^{0.333}}, \quad (23)$$

$$y \equiv \left[\frac{M}{10^{12} h^{-1} M_\odot} \right]^{-1}.$$

Figure 10 shows the evolution of $c_{\min}$ and $\sigma_{\min}^{-1}$ with "time" x, and presents the approximations given in eqs.(19-20). The evolution is clearly related with the transition from the matter dominated period ($\Omega_m(a) \approx 1$, $x < 0.3$) to the Λ-dominated one with $x > 0.7$. Approximations for the halo concentration are presented in Figure 8 for some redshifts. The parameters A, b, c, d of the $\mathcal{C}(\sigma')$ relation are determined from the best fit to the concentration–$\sigma(M)$ Bolshoi/MultiDark data at all redshifts.

Here is a step-by-step description how to estimate halo concentration:

- For given mass M and $a = 1/(1 + z)$ find x, $D(a)$, and $\sigma(M, a)$ using eqs. (13, 12, 16 or 23)
- Use eq. (18) to find parameters B_0 and B_1.
- Use eqs. (15-16) to find σ' and $\mathcal{C}$
- Use eq. (14) to find halo concentration $c(M, z)$.

We present the final results and approximations in two different forms. Functions B_0 and B_1 can be used to find values of $\mathcal{C}$ and σ', which is effectively the same as rescaling concentrations $c(\sigma, x)$ measured in simulations to the
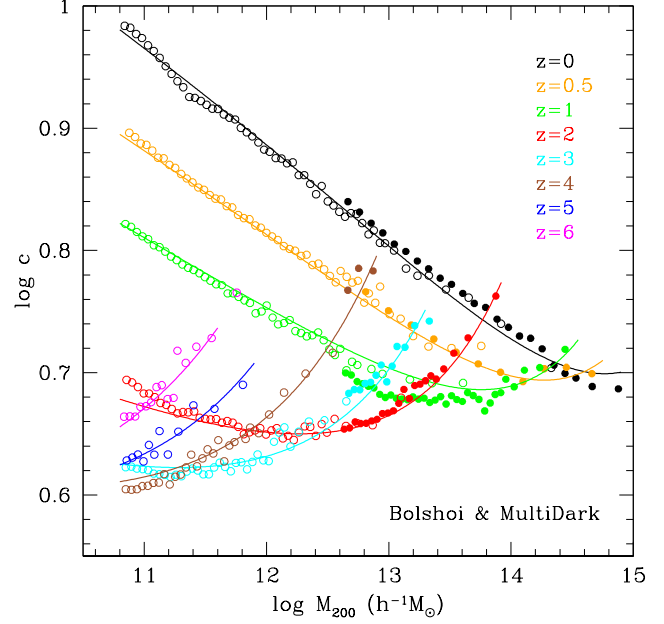

Figure 12. Halo mass–concentration relation of distinct halos at different redshifts in the Bolshoi (open symbols) and MultiDark (filled symbols) simulations is compared with analytical approximation eqs.(14-16 (curves)). The errors of the approximation are less than a few percent.

same redshift $z = 0$. Figure 11 shows results of simulations rescaled in this way. The U-shape of $\mathcal{C}(\sigma')$ is clearly seen. The $\mathcal{C}(\sigma')$ function to some degree plays the same role for concentrations as the function $f(\sigma)$ for the mass function in eqs.(3-4). It tells us that there is little evolution in the dependence of concentration with mass once intrinsic scalings (e.g., x instead of expansion parameter) are taken into account.

Another way of showing the approximations is simply plot eqs. (14-16) for different redshifts and compare the results with the median concentration - mass relation in our simulations. This comparison is presented in Figure 12. It shows that the errors of the approximation are just a few percent for the whole span of masses and redshifts.

6   SUMMARY AND CONCLUSIONS

We study the halo concentrations in the ΛCDM cosmology, from the present up to redshift ten, over a large range of scales going from halos similar to those hosting dwarf galaxies to massive galaxy clusters, i.e. halo maximum circular velocities ranging from 25 to 1800 km s^{-1} (about six orders of magnitude in mass), using cosmological simulations with high mass resolution over a large volume. The results presented in this paper are based on the Bolshoi, MultiDark, and Millennium-I and II simulations. There is a good consistency among the different simulation data sets despite the different codes, numerical algorithms, and halo/subhalo finders used in our analysis.

The approximations given here for the evolution of the halo concentration constitute the state-of-the-art of our current knowledge of this basic property of dark matter halos
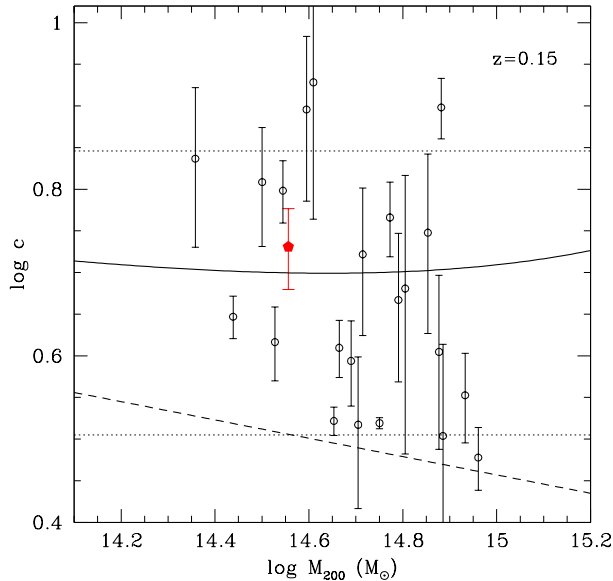
Figure 13. Comparison of observed cluster concentrations (data points with error bars) with the prediction of our model for median halo concentration of cluster-size halos (full curve). Dotted lines show 10% and 90% percentiles. Open circles show results for X-ray luminous galaxy clusters observed with XMM-Newton in the redshift range 0.1-0.3 (Ettori et al. 2010). The pentagon presents galaxy kinematic estimate for relaxed clusters by Wojtak & Łokas (2010). The dashed curve shows prediction by Macciò, Dutton, & van den Bosch (2008), which significantly underestimates the concentrations of clusters.

found in N-body ΛCDM simulations. Naturally, new simulations that improve mass resolution in even larger volumes are needed to face the challenges imposed by current and future observational programs. Our analysis can also be useful for comparison with analytical works that aim to understand the statistics and structural properties of dark matter halos in the standard ΛCDM cosmology.

It is interesting to compare these results with other simulations and models in the literature. Zhao et al. (2003, 2009) were the first to find that the concentration flattens at large masses and at high redshifts. Actually, figure 15 in Zhao et al. (2009) also shows an upturn in concentration at $z = 4$. However, the authors do not even mention it in the text. In addition, their model prediction of the halo mass–concentration relation, based on the halo mass accretion histories, failed to reproduce the upturn behavior of the concentration with increasing mass.

For $M_{\rm vir} = 10^{12}h^{-1}M_\odot$ in the MS-II and Aquarius simulations Boylan-Kolchin et al. (2009) give concentration of $c_{\rm vir} = 12.9$, which is 1.3 times larger than what we get from Bolshoi. Most of the differences are likely due to the larger amplitude of cosmological fluctuations in MS simulations because of the combination of a larger σ_8 and a steeper spectrum of fluctuations. On larger masses Neto et al. (2007) give the following approximation for all halos for MS cosmological parameters: $c_{200} = 7.75(M_{200}/10^{12}h^{-1}M_\odot)^{-0.11}$. Thus, the MS-I has a small ($\sim$10%) difference in c_{200} as compared with our results for $M_{\rm vir} = 10^{14} - 10^{15}h^{-1}M_\odot$.

If we use the same selection conditions (all ha-

los selected by mass) and use the same cosmological model as in Macciò, Dutton, & van den Bosch (2008), then the concentrations of Milky-Way-size halos ($M_{200} = 10^{12}h^{-1}M_\odot$ in Macciò, Dutton, & van den Bosch (2008) are 10% lower than what we find – a reasonable agreement. However, our results are in contradiction with those of Macciò, Dutton, & van den Bosch (2008) when we consider clusters of galaxies. For example, for $M_{200} = 5 \times 10^{14}h^{-1}M_\odot$ we find $c_{200} = 4.6$ while approximations in Macciò, Dutton, & van den Bosch (2008) give a substantially lower value of $c_{200} = 3.1$ – a 50% smaller value.

In Figure 13 we compare predictions of our model eqs.(14-16) for the median mass–concentration relation for galaxy clusters (solid line) with observational estimates obtained from state-of-the-art estimates based on X-ray (Ettori et al. 2010) and kinematic (Wojtak & Łokas 2010) data. The model has been computed at redshift $z = 0.15$, the median of the redshift distribution of the X-ray sample. Open circles are c–M_{200} measurements for the sample of 23 X-ray luminous galaxy clusters observed with XMM-Newton in the redshift range 0.1-0.3 selected from Table 2 in Ettori et al. (2010). We adopted for each cluster an average concentration obtained from both concentration measurements using two different techniques applied by the authors to recover the gas and dark matter profiles. We rejected those clusters where their concentration estimates differs more than 30% between both mass reconstruction techniques. The mass-concentration mean estimate from the kinematic analysis of the combined sample of 41 nearby clusters is also shown as a pentagon symbol (Wojtak & Łokas 2010). The original estimate of Wojtak & Łokas (2010) has been corrected to our overdensity definition. Our model prediction is in good agreement with the mass–concentration observational measurements. Yet, the median halo mass-concentration relation from Maccio et al. 2008 (dashed line) produces by far lower estimates of the concentration for a given value of the halo mass as compared to the observational data.

Our main results can be summarized as follows:

• Our study of the evolution of the $V_{\rm max}/V_{200}$ velocity ratio (which is a measure of concentration) as a function of halo mass M_{200} has confirmed that the halo mass–concentration relation shows a novel feature at high redshifts: a flattening and an upturn at the high-mass end.

• When expressed in terms of the variable $\log \sigma^{-1}$, the halo concentration is a well-behaved function with a U-shaped trend: at small masses the concentration first declines, reaches a minimum at $\log \sigma^{-1} \sim 0.15$, and then increases again at larger masses. The $c - \sigma$ relation is much narrower than the traditional $c(M, z)$ relation, but it is not exactly universal: there are some small dependences with redshift and cosmology.

• The median concentration–$\sigma(M_{200})$ relation can be accurately parameterized by eqs.(14-16). This relation provides an analytical model of the halo mass–concentration median relation $c(M_{200})$ that reproduces all the relevant features, namely the decline of concentration with mass, and its flattening and upturn at high redshift/mass.

• Our estimates for concentration of cluster-size halos are compatible with the recent observational results

and are substantially – a factor of 1.5 – larger than in Macciò, Dutton, & van den Bosch (2008).

REFERENCES

Alam, S. M. K., Bullock, J. S., & Weinberg, D. H. 2002, ApJ, 572, 34

Avila-Reese, V., Firmani, C., Klypin, A., & Kravtsov, A. V. 1999, MNRAS, 310, 527

Boylan-Kolchin M., Springel V., White S. D. M., Jenkins A., 2010, MNRAS, 406, 896

Boylan-Kolchin M., Springel V., White S. D. M., Jenkins A., Lemson G., 2009, MNRAS, 398, 1150

Bryan, G. L., & Norman, M. L. 1998, ApJ, 495, 80

Bullock J. S., Kolatt T. S., Sigad Y., Somerville R. S., Kravtsov A. V., Klypin A. A., Primack J. R., Dekel A., 2001, MNRAS, 321, 559

Cohn J. D., White M., 2008, MNRAS, 385, 2025

Conroy C., Wechsler R. H., Kravtsov A. V., 2006, ApJ, 647, 201

Davis M., Efstathiou G., Frenk C. S., White S. D. M., 1985, ApJ, 292, 371

Dalal N., Lithwick Y., Kuhlen M., 2010, arXiv, arXiv:1010.2539

Eke V. R., Navarro J. F., Steinmetz M., 2001, ApJ, 554, 114

Ettori S., Gastaldello F., Leccardi A., Molendi S., Rossetti M., Buote D., Meneghetti M., 2010, A&A, 524, A68

Evrard A. E., et al., 2002, ApJ, 573, 7

Gao L., Navarro J. F., Cole S., Frenk C. S., White S. D. M., Springel V., Jenkins A., Neto A. F., 2008, MNRAS, 387, 536

Gottloeber, S., & Klypin, A. 2008, in "High Performance Computing in Science and Engineering Garching/Munich 2007", Eds. S. Wagner et al, Springer, Berlin 2008 (arXiv:0803.4343)

Guo, Q., et al. 2011, MNRAS, 164

Hu, W., & Kravtsov, A. V. 2003, ApJ, 584, 702

Hoffman Y., Romano-Díaz E., Shlosman I., Heller C., 2007, ApJ, 671, 1108

Jenkins A., Frenk C. S., White S. D. M., Colberg J. M., Cole S., Evrard A. E., Couchman H. M. P., Yoshida N., 2001, MNRAS, 321, 372

Klypin A., Holtzman J., 1997, astro, arXiv:astro-ph/9712217

Klypin, A., Zhao, H., & Somerville, R. S. 2002, ApJ, 573, 597

Klypin, A., Valenzuela, O., Colín, P., & Quinn, T. 2009, MNRAS, 398, 1027

Klypin A., Trujillo-Gomez S., Primack J., 2010, arXiv, arXiv:1002.3660

Kravtsov, A. V., Klypin, A. A., & Khokhlov, A. M. 1997, ApJ Suppl., 111, 73

Kravtsov, A. V. 1999, Ph.D. Thesis

Lu Y., Mo H. J., Katz N., Weinberg M. D., 2006, MNRAS, 368, 1931

Lukić Z., Heitmann K., Habib S., Bashinsky S., Ricker P. M., 2007, ApJ, 671, 1160

Macciò A. V., Dutton A. A., van den Bosch F. C., 2008, MNRAS, 391, 1940

Navarro J. F., Frenk C. S., White S. D. M., 1997, ApJ, 490, 493

Navarro, J. F., et al. 2004, MNRAS, 349, 1039

Navarro, J. F., et al. 2010, MNRAS, 402, 21

Neto A. F., et al., 2007, MNRAS, 381, 1450

Muñoz-Cuartas J. C., Macciò A. V., Gottlöber S., Dutton A. A., 2010, MNRAS, 1685

Reed D., Governato F., Verde L., Gardner J., Quinn T., Stadel J., Merritt D., Lake G., 2005, MNRAS, 357, 82

Reed D. S., Bower R., Frenk C. S., Jenkins A., Theuns T., 2007, MNRAS, 374, 2

Salvador-Solé E., Manrique A., González-Casado G., Hansen S. H., 2007, ApJ, 666, 181

Sheth R. K., Tormen G., 2002, MNRAS, 329, 61

Springel V., White S. D. M., Tormen G., Kauffmann G., 2001, MNRAS, 328, 726

Springel V., et al., 2005, Nature, 435, 629

Romano-Díaz E., Hoffman Y., Heller C., Faltenbacher A., Jones D., Shlosman I., 2007, ApJ, 657, 56

Tinker J., Kravtsov A. V., Klypin A., Abazajian K., Warren M., Yepes G., Gottlöber S., Holz D. E., 2008, ApJ, 688, 709

Trujillo-Gomez S., Klypin A., Primack J., Romanowsky A. J., 2010, arXiv, arXiv:1005.1289

Warren M. S., Abazajian K., Holz D. E., Teodoro L., 2006, ApJ, 646, 881

Wechsler R. H., Bullock J. S., Primack J. R., Kravtsov A. V., Dekel A., 2002, ApJ, 568, 52

White M., 2001, A&A, 367, 27

Wojtak R., Łokas E. L., 2010, MNRAS, 408, 2442

Zhao D. H., Mo H. J., Jing Y. P., Börner G., 2003, MNRAS, 339, 12

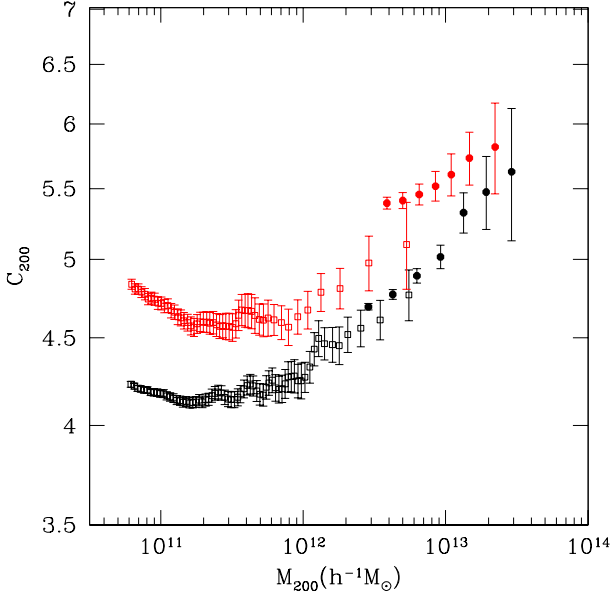Zhao D. H., Jing Y. P., Mo H. J., Börner G., 2009, ApJ, 707, 354

Figure 14. Effects of relaxation on halo concentration at redshift $z = 2$. Top symbols show only relaxed halos. Concentrations of all halos are shown by bottom symbols. Relaxed halos are more concentrated and, just as all halos, show an upturn at large masses. Open symbols show results from the Bolshoi simulation; filled symbols are for the Multidark simulation. Halos are binned by $V_{\rm max}$. The average halo mass M_{200} for each velocity bin is shown on the horizontal axis.

7 APPENDIX: EFFECTS OF HALO SELECTION

Selection of halos has some impact on estimates of halo concentrations. There are different ways to select halos and each selection condition has its own effect. One of the possibilities is to select quiet halos from a population of all halos. Halos can be selected by mass or by the maximum circular velocity $V_{\rm max}$, as we do in this paper. Halo radius may also be defined differently, which substantially changes the halo concentration. Here we consider and discuss the impact of different selection effects.

The selection conditions used in the main part of this paper are: (1) all halos regardless of their relaxation status; (2) overdensity limit of 200 relative to the critical density in eq.(2) defines the radius of a halo. In the main part of the paper we use notation c for concentrations defined in this way. In the Appendix we also use another definition of the virial radius. So, in order to distinguish these two definitions we will use c_{200} for the overdensity 200 definition and $c_{\rm vir}$ for the radius defined by the solution of the top-hat collapse model in the ΛCDM cosmology as approximated by Bryan & Norman (1998). For the parameters of the Bolshoi and MultiDark simulations $\Delta_{\rm vir} = 97$ at $z = 0$. Relative to the matter density this corresponds to $\tilde{\Delta} = \Delta/\Omega_{\rm matter} = 360$.

One of the interesting features in halo concentration is the upturn in concentrations at very large masses. Because the largest halos also grow very fast, one may wonder whether the upturn is just a non-equilibrium feature. We address this issue by comparing concentrations of all halos with the concentrations of only relaxed halos at $z = 2$.

Results presented in Figure 14 show that concentrations of relaxed halos are larger than for all halos by about 10% and more importantly that the upturn is also clearly present in relaxed halos.

In Figure 15 we investigate effects of selection by mass, effects of radius definition, and effects of relaxation at $z = 0$. On both panels the bottom curves are for all halos selected by mass and the top curves are for relaxed halos selected by $V_{\rm max}$. For the latter we show average mass for halos selected by velocities. Results for all halos selected by $V_{\rm max}$ are in between the two curves and are not shown to avoid crowding. In agreement with previous results (e.g., Neto et al. 2007; Macciò, Dutton, & van den Bosch 2008), we find that concentrations of relaxed halos are larger than those of all halos. For smaller masses $M < 10^{13} h^{-1} M_\odot$ the two concentrations have nearly the same slopes and differ by $\sim 7 - 10\%$. The difference increases at larger masses where the concentration of relaxed halos practically stops declining at $M \approx 10^{15} h^{-1} M_\odot$.

The following approximations provide fits for halo concentrations at $z = 0$ for masses $M = 5 \times 10^{10} - 10^{15} h^{-1} M_\odot$:
Relaxed halos selected by $V_{\rm max}$:

$$c_{200} = 7.80 \left(\frac{M_{200}}{10^{12} h^{-1} M_\odot} \right)^{-0.08} \left[1 + 0.2 \left(\frac{M_{200}}{10^{15} h^{-1} M_\odot} \right)^{1/2} \right] \tag{24}$$

$$c_{\rm vir} = 10.5 \left(\frac{M_{\rm vir}}{10^{12} h^{-1} M_\odot} \right)^{-0.08} \left[1 + 0.15 \left(\frac{M_{\rm vir}}{10^{15} h^{-1} M_\odot} \right)^{1/2} \right] \tag{25}$$

All halos selected by halo mass:

$$c_{200} = 7.28 \left(\frac{M_{200}}{10^{12} h^{-1} M_\odot} \right)^{-0.074} \tag{26}$$

$$c_{\rm vir} = 9.7 \left(\frac{M_{\rm vir}}{10^{12} h^{-1} M_\odot} \right)^{-0.074} \tag{27}$$

In summary, we find that different selection criteria work very differently: some are important and some are not:

• Differences in concentrations due to selection of halos by mass or by $V_{\rm max}$ are small at small masses: for $M_{200} < 10^{13} h^{-1} M_\odot$ halos selected by $V_{\rm max}$ have concentrations larger only by a factor $1.02 - 1.04$. The differences somewhat increase at larger masses: at $M_{200} = 5 \times 10^{14} h^{-1} M_\odot$ the difference is a factor of 1.08.

• As expected, the overdensity threshold (in our case either $200\rho_{\rm cr}$ or the virial overdensity) has a large impact on halo concentration. We find that at $z = 0$ the ratio of the concentrations is nearly independent on halo mass: $c_{\rm vir}/c_{200} = 1.35$. This is consistent with previous results (e.g. Macciò, Dutton, & van den Bosch 2008). Note that one may naively expect that there should be a mass-dependent correction due the change in the overdensity threshold (Hu & Kravtsov 2003). However, this is only true for a toy model of an isolated halo with the NFW density profile. In reality, the situation is more complex and there are two effects: one due to the fact that the same halo is measured at different radii and another due to the difference in the sets of halos: some of distinct halos defined by small R_{200} radius cease to be distinct and become subhalos for large virial radius.
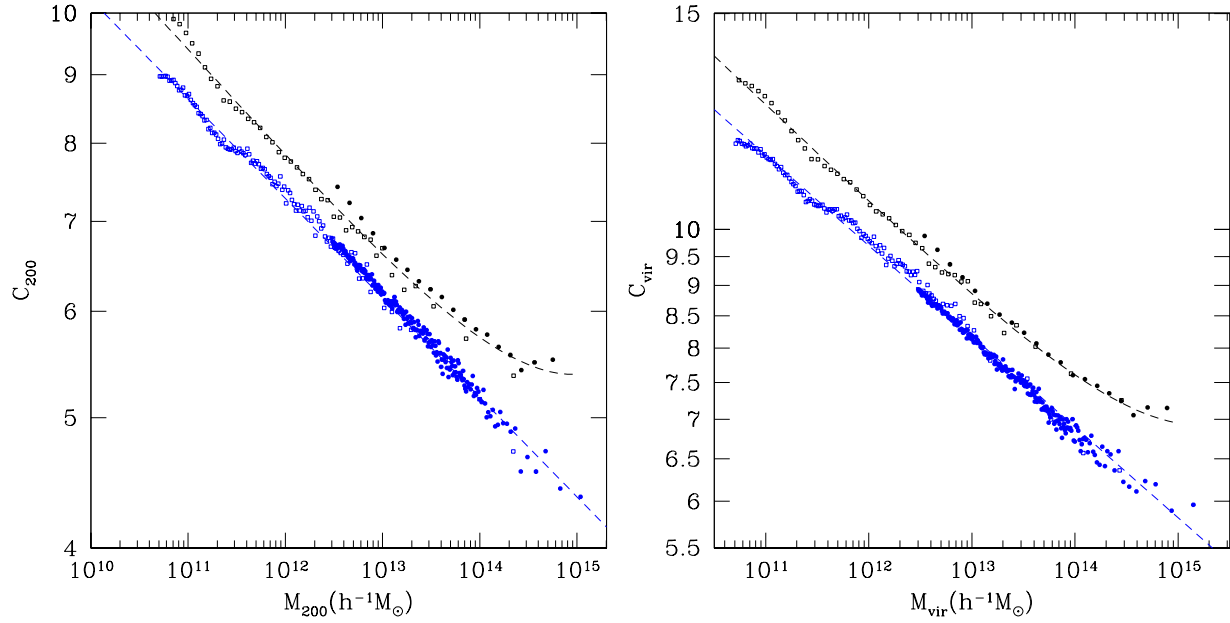
Figure 15. Effects of halo selection. The left panel shows results for the overdensity 200 values; the right panel is for the virial overdensity. Bottom symbols and curves show concentrations for all halos selected by mass. The top symbols and curves are for relaxed halos selected by maximum circular velocity. Open symbols show results from the Bolshoi simulation; filled symbols are for the Multidark simulation. All halos selected by V_{max} are in between the two sets of curves.

• Halos with large masses are effected the most by a particular choice of halo selection. For example, Figure 15 indicates that the concentration c_{200} of relaxed halos selected by V_{max} is 20 percent larger than that of all halos selected by mass for $M_{200} = 10^{15} h^{-1} M_\odot$.

This paper has been typeset from a TeX/ LaTeX file prepared by the author.